

UNIVERSITY OF BIRMINGHAM

Research at Birmingham

Stochastic backscatter modelling for the prediction of pollutant removal from an urban street canyon: a large-eddy simulation

O'Neill, James; Cai, Xiaoming; Kinnersley, Robert

DOI:

[10.1016/j.atmosenv.2016.07.024](https://doi.org/10.1016/j.atmosenv.2016.07.024)

License:

Creative Commons: Attribution-NonCommercial-NoDerivs (CC BY-NC-ND)

Document Version

Peer reviewed version

Citation for published version (Harvard):

O'Neill, J, Cai, X & Kinnersley, R 2016, 'Stochastic backscatter modelling for the prediction of pollutant removal from an urban street canyon: a large-eddy simulation', *Atmospheric Environment*, vol. 142, pp. 9-18.
<https://doi.org/10.1016/j.atmosenv.2016.07.024>

[Link to publication on Research at Birmingham portal](#)

Publisher Rights Statement:

Checked for eligibility: 15/08/2016

General rights

Unless a licence is specified above, all rights (including copyright and moral rights) in this document are retained by the authors and/or the copyright holders. The express permission of the copyright holder must be obtained for any use of this material other than for purposes permitted by law.

- Users may freely distribute the URL that is used to identify this publication.
- Users may download and/or print one copy of the publication from the University of Birmingham research portal for the purpose of private study or non-commercial research.
- User may use extracts from the document in line with the concept of 'fair dealing' under the Copyright, Designs and Patents Act 1988 (?)
- Users may not further distribute the material nor use it for the purposes of commercial gain.

Where a licence is displayed above, please note the terms and conditions of the licence govern your use of this document.

When citing, please reference the published version.

Take down policy

While the University of Birmingham exercises care and attention in making items available there are rare occasions when an item has been uploaded in error or has been deemed to be commercially or otherwise sensitive.

If you believe that this is the case for this document, please contact UBIRA@lists.bham.ac.uk providing details and we will remove access to the work immediately and investigate.

1 **Stochastic backscatter modelling for the prediction of pollutant removal from an**
2 **urban street canyon: a large-eddy simulation**

3 J.J. O'Neill^a, X.-M. Cai^{a*} and R. Kinnersley^b

4 ^aSchool of Geography, Earth and Environmental Sciences, University of Birmingham, UK

5 ^bEnvironment Agency, Bristol, UK

6 *Corresponding author: X.-M. Cai, School of Geography, Earth and Environmental Sciences,
7 University of Birmingham, Edgbaston, Birmingham, B15 2TT. Email: x.cai@bham.ac.uk

8 **Abstract**

9 The large-eddy simulation (LES) approach has recently exhibited its appealing capability of
10 capturing turbulent processes inside street canyons and the urban boundary layer aloft, and its
11 potential for deriving the bulk parameters adopted in low-cost operational urban dispersion
12 models. However, the thin roof-level shear layer may be under-resolved in most LES set-ups
13 and thus sophisticated subgrid-scale (SGS) parameterisations may be required. In this paper,
14 we consider the important case of pollutant removal from an urban street canyon of unit
15 aspect ratio (i.e. building height equal to street width) with the external flow perpendicular to
16 the street. We show that by employing a stochastic SGS model that explicitly accounts for
17 backscatter (energy transfer from unresolved to resolved scales), the pollutant removal
18 process is better simulated compared with the use of a simpler (fully dissipative) but widely-
19 used SGS model. The backscatter induces additional mixing within the shear layer which acts
20 to increase the rate of pollutant removal from the street canyon, giving better agreement with
21 a recent wind-tunnel experiment. The exchange velocity, an important parameter in many
22 operational models that determines the mass transfer between the urban canopy and the
23 external flow, is predicted to be around 15% larger with the backscatter SGS model;

24 consequently, the steady-state mean pollutant concentration within the street canyon is
25 around 15% lower. A database of exchange velocities for various other urban configurations
26 could be generated and used as improved input for operational street canyon models.

27 **Keywords:** Large-eddy simulation; Roof-level shear layer; Stochastic backscatter modelling;
28 Street canyon; Urban canopy air pollution.

29 **1. Introduction**

30 With over half of the world's population living in urban areas (WHO, 2015), it is important to
31 understand the effects of the densely built environment on the transportation and dispersion
32 of pollutants emitted near ground-level. Street canyons form a key constituent part of the
33 urban fabric (Oke, 1988), and particular concern surrounds the case of vehicular emissions
34 released within deep street canyons (i.e. $H/W \gtrsim 0.7$, where H is the building height and W is
35 the street width), in which a 'skimming flow' regime is established (Oke, 1987). In this
36 regime, the bulk of the flow passes over the street canyon, leaving pollutants largely trapped
37 within the canyon and thus susceptible to build up to potentially harmful levels. An extreme
38 case occurs when the oncoming wind is exactly perpendicular to the street axis, which has
39 been observed to lead to particularly poor ventilation, and thus poor air quality (DePaul and
40 Sheih, 1985; Xie et al., 2003).

41 The associated risks to human health have led to an extensive number of controllable
42 (idealised) experiments being attempted in order to better understand wind flow and
43 dispersion characteristics for the perpendicular skimming flow regime. These experiments
44 include reduced-scale wind-tunnel (Meroney et al., 1996; Kastner-Klein and Plate, 1999;
45 Pavageau and Schatzmann, 1999; Brown et al., 2000; Simoëns and Wallace, 2008; Salizzoni
46 et al., 2009; Blackman et al., 2015) and water-channel (Baik et al., 2000; Li et al., 2008; Di
47 Bernardino et al., 2015) testing, as well as numerical computational fluid dynamic (CFD)

48 modelling (Baik and Kim, 1999, 2002; Liu and Barth, 2002; Walton and Cheng, 2002; Cui et
49 al., 2004; Li et al., 2005; Liu et al., 2005; Cai et al., 2008; Cheng and Liu, 2011; Michioka et
50 al., 2011; Cai, 2012; Liu and Wong, 2014). CFD models offer a number of advantages over
51 laboratory experiments, including lower set-up and running costs, significantly better spatial
52 coverage, and the ability to test a variety of urban configurations with relative ease. They
53 typically fall into one of two categories: Reynolds-averaged Navier-Stokes (RANS) models,
54 which parameterise all turbulence length-scales in search of the mean flow and dispersion
55 patterns; and large-eddy simulation (LES) models, which parameterise only the smallest
56 turbulence length-scales (whilst resolving the larger scales) and retrieve the mean spatial
57 patterns by time-averaging the instantaneous model output record (Vardoulakis et al., 2003;
58 Li et al., 2006). LES is computationally more expensive than RANS but offers greater
59 simulation accuracy. For example, Walton and Cheng (2002) compared the performance of
60 RANS and LES for simulating pollutant dispersion in a street canyon of unity aspect ratio (i.e.
61 $H/W = 1$) and found the LES-predicted mean concentration patterns to be in much better
62 agreement with wind-tunnel data. This was due to the model's ability to capture important
63 unsteadiness in the canyon's primary recirculating vortex, which was observed to lead to
64 puffs of pollution being intermittently ejected from the canyon rather than being steadily
65 dispersed away, as simulated by RANS. The dominating influence of intermittent events on
66 tracer release from a street canyon was also observed in the wind-tunnel experiment of
67 Simoëns and Wallace (2008), who concluded that a simple mean concentration gradient
68 model applied to the Reynolds-averaged transport equation would be insufficient to model
69 scalar fluxes. The importance of capturing unsteadiness in simulations of dispersion around
70 buildings has also been demonstrated in other LES-RANS comparison studies, e.g. Dejoan et
71 al. (2010), Tominaga and Stathopoulos (2010), Salim et al. (2011a), Salim et al. (2011b).

72 LES is thus better suited to derive input parameters for simpler operational street canyon
73 models, which is recently being attempted (e.g., the DIPLOS project – <http://www.diplos.org>).

74 To achieve adequate simulation accuracy with LES, the choice subgrid-scale (SGS) model,
75 which parameterises the effects of the unresolved scales of motion on the resolved ones, is
76 often critical (Mason, 1994). This is particularly true in under-resolved flow regions where
77 the small-scale motions carry an appreciable fraction of the turbulent energy. For street
78 canyon flow, Letzel et al. (2008) showed that Kelvin Helmholtz waves generated within the
79 roof-level shear layer significantly affect the behaviour of a dispersing tracer. However, with
80 substantially fine resolution (at least 100 across-canyon grid points) required to explicitly
81 resolve these waves, much of the shear layer dynamics is often unavoidably handled by the
82 SGS model. This poses a significant challenge to even the most complex SGS models
83 available. O'Neill et al. (2016) argued that backscatter (transitory transfer of turbulent kinetic
84 energy from unresolved to resolved scales by eddy interactions that produce larger
85 wavelengths) is an important process within the roof-level shear layer that should therefore
86 be explicitly considered in the SGS model. Use of the popular Smagorinsky (1963) SGS
87 model, which only parameterises forward energy transfer (i.e. it is fully dissipative), has been
88 found to under-predict the primary vortex strength inside the street canyon (Cui et al., 2004).

89 With the dynamic SGS model (Germano et al., 1991; Lilly, 1992), which only accounts for
90 partial backscatter through locally reduced eddy-viscosities (strong backscatter requires
91 negative values, which are typically prohibited), similar deficiencies can also be observed
92 (Cheng and Liu, 2011; Liu and Wong, 2014). Alternatively, O'Neill et al. (2016) employed a
93 SGS model that explicitly accounts for backscatter using a stochastic forcing term in the
94 momentum equation (Mason and Thomson, 1992). This increased the momentum transfer
95 across the shear layer, thus driving an intensification of the primary vortex, bringing it
96 significantly closer towards wind-tunnel observations (Brown et al., 2000).

97 The next step, and the aim of the present paper, is to test what effect the backscatter model
98 has on the prediction of pollutant removal from the street canyon. To achieve this, we
99 compare LES output from two separate simulations of scalar transport in a street canyon of
100 unit aspect ratio; one adopting the Smagorinsky SGS model, and the other adopting the
101 stochastic backscatter SGS model. The paper is structured as follows. Section 2 provides a
102 mathematical overview of the LES methodology, as well as the two different SGS models
103 adopted in this study (the Smagorinsky model and the stochastic backscatter model). Section
104 3 describes the LES model configuration settings for each simulation. We then present the
105 results and discuss the implications in Section 4. Finally, conclusions are drawn in Section 5.

106 **2. Mathematical formulation**

107 **2.1. LES overview**

108 LES numerically solves the filtered Navier–Stokes and continuity equations on a discretised
109 grid. The filter separates the larger eddies, which are resolved by the model, from the smaller
110 eddies, which are not resolved and must therefore be parameterised. For an incompressible
111 fluid, the governing equations (using tensor notation) are given by:

$$\frac{\partial u_i}{\partial t} + u_j \frac{\partial u_i}{\partial x_j} = -\frac{1}{\rho} \frac{\partial p}{\partial x_i} - \frac{\partial \tau_{ij}}{\partial x_j}, \quad (1)$$

$$\frac{\partial u_i}{\partial x_i} = 0, \quad (2)$$

112 where u_i is the filtered (resolved) velocity component in the direction x_i , p is the filtered
113 pressure, t is time, ρ is the (constant) air density, τ_{ij} is the turbulent SGS stress tensor, and
114 where viscous effects have been assumed to be negligible compared with the turbulent SGS
115 stresses for the large Reynolds number flow. The term involving τ_{ij} represents the effects of
116 the unresolved velocity field on the resolved field, and is handled by the SGS model.

117 In addition, the filtered transport equation can be solved to represent the dispersion of a
 118 passive scalar:

$$\frac{\partial C}{\partial t} + u_j \frac{\partial C}{\partial x_j} = -\frac{\partial \sigma_i}{\partial x_i} + S, \quad (3)$$

119 where C is the filtered scalar field, S is a source term, and σ_j are the SGS scalar fluxes, which
 120 again must be handled by the SGS model.

121 2.2. Smagorinsky SGS model

122 The net effect of the unresolved turbulent stresses is to drain energy from the resolved flow
 123 (forward energy transfer) to the SGS field. The Smagorinsky SGS model is a purely
 124 dissipative model that seeks to parameterise this net energy transfer using a subgrid-scale
 125 eddy-viscosity, ν_{sgs} , in an analogous way to molecular diffusion:

$$\tau_{ij} - \frac{1}{3} \delta_{ij} \tau_{kk} = -2\nu_{\text{sgs}} S_{ij}, \quad (4)$$

$$S_{ij} = \frac{1}{2} \left(\frac{\partial u_i}{\partial x_j} + \frac{\partial u_j}{\partial x_i} \right), \quad (5)$$

$$\nu_{\text{sgs}} = (C_S \Delta)^2 \sqrt{2S_{ij} S_{ij}}, \quad (6)$$

126 where δ_{ij} is the Kronecker delta, C_S is the so-called Smagorinsky constant, and $\Delta =$
 127 $(\Delta x \Delta y \Delta z)^{1/3}$ is the local grid-scale (i.e. the arithmetic mean of the three local grid spacings
 128 in x , y , and z , which define a three-dimensional Cartesian coordinate system). The isotropic
 129 part of the SGS stresses ($1/3 \delta_{ij} \tau_{kk}$) is absorbed into the pressure gradient term in Eq. (2).
 130 Similarly, the SGS scalar fluxes are modelled using an eddy-diffusivity, α_{sgs} :

$$\sigma_i = -\alpha_{\text{sgs}} \frac{\partial C}{\partial x_i}, \quad (7)$$

$$\alpha_{\text{sgs}} = \frac{\nu_{\text{sgs}}}{Sc}, \quad (8)$$

131 where Sc is the Schmidt number. Despite known deficiencies, the Smagorinsky model is
 132 often adequate in many simple flows, and remains the most popular choice for SGS
 133 modelling due, in part, to its computationally low cost.

134 **2.3. Stochastic backscatter SGS model**

135 The net drain of energy from resolved to unresolved scales is in fact the result of many events
 136 of forward energy transfer (or ‘forward-scatter’) and reverse energy transfer (or ‘backscatter’).
 137 Backscatter SGS models seek to represent the energy transfer in both directions separately
 138 and, as such, are better suited to situations in which the residual drain of energy near the cut-
 139 off scale is small compared with the separate forward-scatter and backscatter of energy. The
 140 stochastic approach pioneered by Mason and Thomson (1992) retains the Smagorinsky model
 141 for the forward-scatter part, but further represents the backscatter part through an additional
 142 semi-random acceleration term, a_i , with zero mean, that is added directly to the filtered
 143 Navier-Stokes equations (Eq. (1)), i.e. $\partial u_i / \partial t = \dots + a_i$. The acceleration fields are
 144 constructed to be divergence-free so that Eq. (2) remains unviolated. These accelerations give
 145 rise to an increase in local turbulent kinetic energy (TKE), and are scaled to ensure that this
 146 rate of TKE input is equal (on average) to the locally expected energy backscatter rate, which
 147 is a function of the local dissipation rate ϵ (Mason and Thomson, 1992):

$$\overline{a_1^2} + \overline{a_2^2} + \overline{a_3^2} = \frac{2C_B}{T_B} \epsilon, \quad (9)$$

148 where the overbar denotes a time-average, C_B is the backscatter coefficient, T_B the
 149 backscatter time-scale (the time between successively generated random acceleration fields),
 150 and where it is assumed that the local turbulence production scale is larger than the local LES
 151 filter scale. In this study, we follow the procedure outlined in O'Neill et al. (2015) and later

152 improved in O'Neill et al. (2016) for generating the backscatter acceleration fields a_i , to
153 which we refer the reader for details. In essence, this stochastic backscatter model allows for
154 local control of the length-scale, anisotropy and vertical momentum flux associated with the
155 backscatter-induced velocity fluctuations.

156 Mason and Thomson (1992) also outlined an analogous approach to model the SGS scalar
157 fluxes, in which the magnitude of backscatter (in this case, of scalar variance rather than TKE)
158 is controlled via the scalar backscatter coefficient, $C_{B\theta}$. However, we have found that the
159 inclusion of scalar backscatter (in addition to energy backscatter) gives insignificant
160 differences in calculated mean statistics when the scalar is a dynamically passive tracer (as
161 opposed to, e.g., temperature, which has a dynamical feedback). For example, the time-
162 averaged quasi-steady pollutant concentration within the street canyon (calculated in Section
163 4.2.1) differs by less than 1% when scalar backscatter is included on top of energy
164 backscatter. We thus choose $C_{B\theta} = 0$, i.e. the SGS scalar fluxes are handled entirely by the
165 Smagorinsky model (Eq. (7)); this further allows us to discern the effects of energy
166 backscatter in isolation.

167 **3. LES model configuration**

168 The LES model used in this study is based on Colorado State University's Regional
169 Atmospheric Modelling System (RAMS), originally developed by Pielke et al. (1992) and
170 later adapted to LES of street canyon flow by Cui et al. (2004). The model uses a scale-
171 independent dynamic core to solve the non-hydrostatic equations on a staggered Arakawa-C
172 grid. The finite-volume discretisation is second-order in space, and uses a flux-conservative
173 leapfrog time differencing method. The model time-step set to $\Delta t = 0.04$ s in our simulations.
174 The computational domain and grid setup used in this study are the same as in O'Neill et al.
175 (2016). The LES domain is also schematised in Figure 1. The coordinate system is aligned

176 such that x points in the positive streamwise direction (with respect to the mean wind above
177 the canyon), y in the spanwise (along-street) direction, and z vertically upwards, with the
178 origin located at the ground-level centre of the street canyon. $L_x, L_y, L_z = 24 \text{ m}, 40 \text{ m}, 94 \text{ m}$
179 define the domain extent in x, y, z , respectively. Constant horizontal grid spacing of $\Delta x =$
180 0.3 m and $\Delta y = 1 \text{ m}$ is used throughout the domain, and the vertical grid spacing is set to
181 $\Delta z = 0.3 \text{ m}$ within the street canyon with a gradual stretching above roof-level up to the
182 domain top.

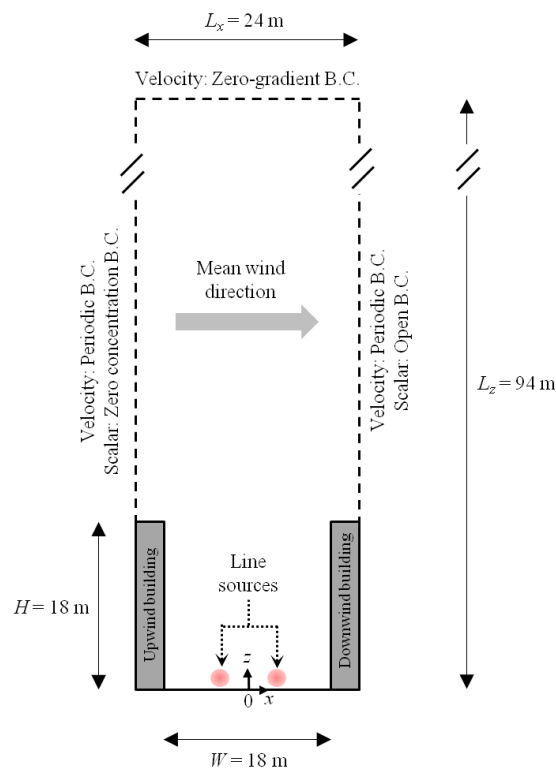
183 The initial wind profile is prescribed as logarithmic above the street canyon (zero velocity
184 inside it) with a maximum of 2.6 m s^{-1} near the domain top. The Reynolds number based on
185 this velocity and H is approximately 3×10^6 . A constant pressure gradient force above roof-
186 level is applied throughout the simulation to approximately conserve the total momentum in
187 the system. The boundary conditions for the velocity field are periodic in the x and y
188 directions, which effectively prescribes an infinitely repeating and infinitely long street
189 canyon. A zero-gradient boundary condition is used for velocity at the top of the domain. A
190 logarithmic boundary condition is used for all grid points adjacent to solid surfaces; this
191 remains the most common choice for LES of atmospheric flows around buildings (e.g.
192 Santiago et al. (2010); Park and Baik (2013); Cheng and Porte-Agel (2015)) despite its
193 limitations, due to the present lack of viable alternatives in the literature.

194 Vehicular emissions from two lanes of traffic are modelled using two slightly elevated line
195 sources running parallel to the y axis along the full length of the street. The first source is
196 located at $(x/W, z/H) = (-1/6, 1/20)$ and the second source at $(x/W, z/H) =$
197 $(1/6, 1/20)$. A passive (neutrally buoyant and chemically inert) scalar is emitted from each
198 source at a constant rate of $Q_s = 500 \mu\text{g m}^{-1} \text{ s}^{-1}$. Each source is given a small finite extent
199 (5 grid points) in x and z , with a two-dimensional (2D) Gaussian concentration profile, in

200 order to minimise issues associated with near-source numerical dispersion. A periodic
 201 boundary condition for the scalar field is employed only in the y direction. An open boundary
 202 condition is used in the x direction (above the street canyon), which corresponds to the
 203 situation in which escaped pollutants leave the downwind boundary and do not re-enter the
 204 upwind boundary, at which a zero background concentration is specified. This is achieved
 205 through the specification of the following conditions at these boundaries:

$$C = 0 \quad \text{at } x = -\frac{L_x}{2}, \quad (10)$$

$$\frac{dC}{dt} + u \frac{dC}{dx} = 0 \quad \text{at } x = \frac{L_x}{2} \quad (11)$$



206 **Figure 1 – Schematic of the LES computational domain (B.C. = boundary condition).**

207 The performances of two SGS models are compared against each other in this study; the
 208 Smagorinsky (SMAG) model and a stochastic backscatter (SB) model (an overview of the
 209 mathematic formulation of each model is given in Section 2). A value of $C_S = 0.1$ is adopted
 210 as the Smagorinsky constant, which has previously been reported to give optimum behaviour

211 in practical LESs of neutrally stratified flows (Mason and Callen, 1986), and has been used in
212 numerous similar studies in the past, e.g. Xie et al. (2004); Boppana et al. (2010); Santiago et
213 al. (2010).

214 The parameters for the SB model are selected based on the analysis of O'Neill et al. (2016).
215 In that study, a systematic assessment of the effects of changing the backscatter coefficient
216 C_B , local backscatter length-scale l_B , and backscatter vertical momentum flux factor VMF_B
217 (both separately and in combination) was performed. Physically, C_B controls the strength of
218 the backscatter 'eddies', l_B controls their characteristic size, and VMF_B controls momentum
219 flux at the grid-scale (by varying the correlation between the backscatter-induced streamwise
220 and vertical velocity fluctuations). Typically, larger values of each parameter facilitate
221 increased mixing across the roof-level shear layer and thus entrain more momentum into the
222 street canyon from the external flow. For each tested parameter set, the strength of the
223 recirculating vortex (primary eddy) within the street canyon was calculated from the resulting
224 mean velocity field, and compared against the primary eddy strength measured in a
225 corresponding wind-tunnel experiment. It was found that the best match was attained with the
226 following values: $C_B = 1.4$; $l_B = \max\{\Delta x_i, \Delta y_j, \Delta z_k\}$, where $\Delta x_i, \Delta y_j$ and Δz_k are the local
227 grid spacings in x, y and z respectively (subscripts i, j and k denote the discrete model grid-
228 point indices); and $VMF_B = 0.5$. Also following our previous paper, the backscatter time-
229 scale is set to $T_B = 2\Delta t$, the backscatter accelerations are prescribed to be isotropic and are
230 only applied to the LES momentum equations within the region $0.8 \leq z/H \leq 1.2$ (the energy
231 backscatter rate is negligible outside this region – see O'Neill et al. (2016) for more details).

232 The model is initially run without any source emissions, for a period of 60 min (around 24
233 primary-eddy turnover times). This gives the flow dynamics sufficient time to reach a quasi-
234 steady state. Source emissions are then started and the model is run for a further 120 min; this

235 gives sufficient time for a quasi-steady state of pollutant transport to be established. Data
236 from the final 30 min of the simulation period are then processed for averaging to obtain the
237 results presented in Section 4, with the exception of Section 4.1, which uses data obtained
238 after further turning off the source and recording subsequent time-series of decaying
239 concentration (further details given therein). Averaging is performed in both time (t) and in
240 the homogeneous spanwise (y) direction.

241 **4. Results and discussion**

242 The present study extends the work of O'Neill et al. (2016), who applied a stochastic
243 backscatter SGS model to LES of street canyon flow and compared dynamical properties
244 against those obtained with the Smagorinsky SGS model, to further consider the effects on
245 pollutant transport. The SB model was previously validated against a wind-tunnel velocity
246 dataset and shown to lead to an improvement over the SMAG model, with a better prediction
247 of the mean streamwise and vertical velocity profiles, and thus the primary eddy recirculation
248 strength, within the canyon. Here, we first attempt to validate the SB model further using a
249 recent wind-tunnel pollution dataset (Section 4.1), which provides further confidence that
250 simulation accuracy is improved over the use of the SMAG model. We then compare other
251 dispersion and transport properties from the two LES (SMAG and SB model) against each
252 other, also comparing qualitatively with results from previous measurement and modelling
253 studies where possible (Sections 4.2–4.3).

254 **4.1. Model validation: Exchange velocity**

255 We first validate the LES output against the wind-tunnel (WT) dataset of Salizzoni et al.
256 (2009), in which the pollutant exchange velocity, v_e , (alternatively the transfer or ventilation
257 velocity) was estimated via ‘wash-out’ curves, i.e. measured time-series of decaying pollutant
258 concentrations after an emissions shutdown. This value is of particular interest to urban

259 dispersion modellers, as it forms the key parameter that describes the pollutant mass transfer
260 between the urban canopy and the flow above it in many simplified operational models.

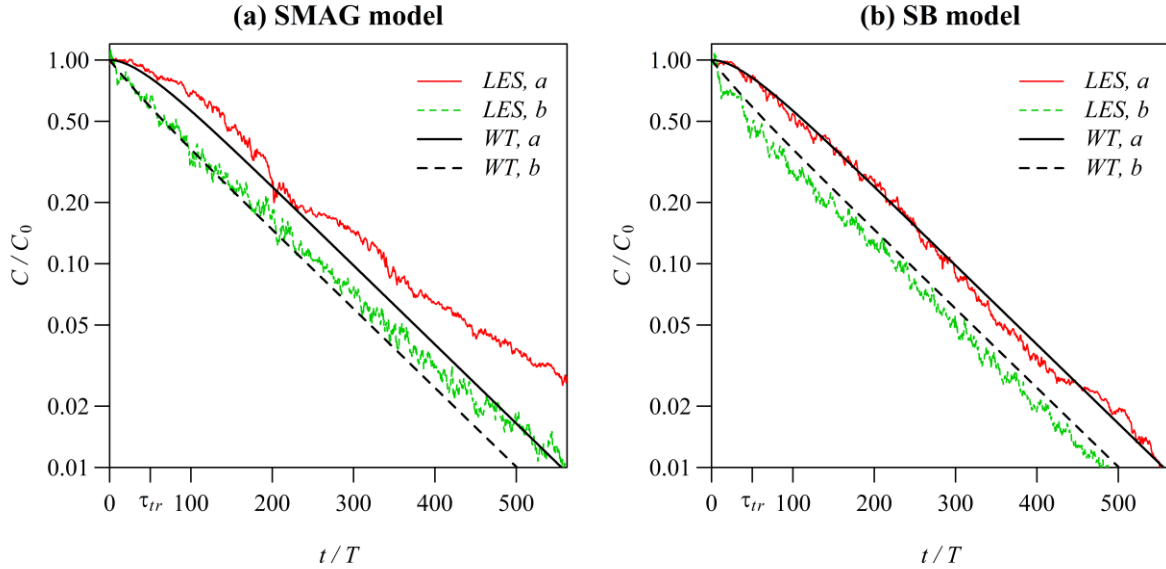
261 The WT test section was 1 m high, 0.7 m wide and 8 m long. Bars with a square cross-section
262 measuring 6×6 cm and spanning the width of the WT were spaced equally apart along the
263 full length of the test-section floor to form repeating street canyons of unit aspect ratio,
264 perpendicular to the direction of wind flow ('Configuration A' in their paper). A fully-
265 developed neutral boundary layer, with thickness $\delta = 0.6$ m and friction velocity $u_* =$
266 0.33 m s^{-1} , was generated using three 0.5 m high spires, placed at the entrance to the test
267 section, and immediately followed by the repeating street canyon blocks. The Reynolds
268 number based on H and (separately) the far-field free-stream velocity U_∞ or the mean velocity
269 at roof-level was approximately 25,000 and 5,000, respectively, both of which exceed the
270 critical value of 3,400 required to ensure negligible viscous effects in WT experiments with
271 an urban roughness (Pavageau and Schatzmann, 1999). Periodic street-canyon flow was
272 ensured by choosing the canyon in which measurements were recorded to be 6 m downwind
273 of the test-section entry point (Salizzoni et al., 2008). Passive tracer gas was released at a
274 constant rate from a porous tube, which ran down the length of the street canyon centre-line
275 in a slot located underneath (and flush with) the canyon floor, to mimic the steady release of
276 vehicular pollution. Once a quasi-steady state of pollutant transport had been reached, the
277 source was turned off. Time-series of decaying pollutant concentration ('wash-out curves')
278 were then recorded over a 5 second period, using flame ionisation detection (FID) with a
279 sampling frequency of 300 Hz, at five separate points within the street canyon: at point a ,
280 located at $(x/W, z/H) = (0, 0)$ (i.e. the street canyon centre-point); and at points b , c , d and
281 e , located at $(x/W, z/H) = (-1/3, 1/2)$, $(0, 5/6)$, $(1/3, 1/2)$ and $(0, 1/6)$, respectively (i.e.
282 each a radial distance of $H/3$ from the centre). The experiment was repeated 50 times and the
283 ensemble-averaged wash-out curve computed at each of these points. Since the curves at

284 points b , c , d and e did not differ significantly from each other, only the curves for points a
285 and b were taken forward. An analytical model was then fitted to these curves¹ to obtain the
286 value for v_e .

287 We record decaying concentrations for each LES in an equivalent manner; however, rather
288 than repeating each simulation 50 times, we calculate the concentration at a particular x, z
289 location and time t by averaging in the homogeneous spanwise (y) direction (a total of 40
290 values). We note that although the LES source configuration is different to that of the WT
291 (two line sources compared with one, and slightly elevated rather than at ground-level), this
292 has negligible effect on the calculated exchange velocity. We also note that the scaled
293 boundary-layer depth in the LES is around half that in the WT experiment (around $5H$
294 compared with $10H$). Although this would certainly effect the comparison of flow statistics
295 near the top of the LES domain, it has been shown in previous large-eddy (Xie and Castro,
296 2006) and direct numerical (Coceal et al., 2006) simulations over building-like obstacles that
297 the domain height *does not* significantly affect the flow within the roughness sublayer and
298 urban canopy, which is where the focus of the present study lies.

299 As the WT wash-out curves in Salizzoni et al. (2009) were reported in absolute time, we must
300 normalise the data to allow for comparison with our simulations. The street canyon height H
301 provides the reference length-scale, and U_∞ provides the reference velocity-scale ($U_\infty =$
302 6.75 m s^{-1} and 2.6 m s^{-1} in the WT and LES, respectively); the reference time-scale T is
303 thus given by H/U_∞ .

¹ A parameter β , describing the relative volumes of the central well-mixed core and outer region of the canyon, was empirically determined by the authors to fall within $0.8 < \beta < 0.9$ prior to fitting the model. In our analysis, we compare with the $\beta = 0.85$ case as it falls at the centre of this range.



304 **Figure 2 – Normalised pollutant wash-out curves at points a (street canyon centre) and**
 305 **b (outer vortex) for the LES with: (a) the SMAG model; (b) the SB model. Darker lines**
 306 **show the normalised analytical model that fits the WT data at each of these points**
 307 **(Salizzoni et al., 2009). τ_{tr} on lower axis denotes the transition period time-scale (see**
 308 **text for details).**

309 Figure 2 shows the pollutant wash-out curves at points a (street canyon centre) and b (outer
 310 vortex) for the LES with: (a) the SMAG model, and; (b) the SB model. Concentrations are
 311 plotted on a logarithmic axis and are normalised by the initial (quasi-steady) concentration at
 312 that given location, C_0 , and time is normalised by T as discussed above. Each plot also shows
 313 the normalised analytical two-box model curves from the WT experiment, which were shown
 314 to fit the measured wash-out curves very well, apart from very early on after the emissions
 315 shutdown due to the measured data being inevitably contaminated by the experimental
 316 settings (see the discussions in Salizzoni et al. (2009)). The numerical experiment does not
 317 suffer from such contamination issues and so the modelled curves can be used to assess our
 318 LES results over the entire time-series. The two boxes in the analytical model represent the
 319 primary eddy core and the recirculating ring outside the core, respectively. The concentration
 320 in the core is represented by the concentration at point a , which we denote by C_a , and the
 321 concentration in the ring by the concentration at point b , which we denote by C_b . The LES
 322 wash-out curves are generally consistent with the WT fitted analytical model, in that there is

323 an initial transient during which C_b drops fast *and* that C_a falls much less rapidly than C_b . As
324 elucidated by Salizzoni et al. (2009), this is due to the fact that the time-scale associated with
325 the turbulent transport of pollutants from the primary eddy core towards the outer ring is
326 slower than the time-scale associated with the removal of pollutants from the top of the
327 primary eddy through the turbulent roof-level shear layer. Our careful examination of the
328 analytical model yields that the time-scale of this transient period, if we denote it by τ_{tr} , is
329 approximately $50T$; when $t \gg \tau_{tr}$, the analytical model gives a solution asymptotically
330 approaching a pure exponential decaying, which appears as a straight line on the log-linear
331 coordinates, as illustrated at later times by the WT curves in Figure 2.

332 In addition, the slope of this straight line (for C_a or C_b – the slopes are identical) can be used
333 to estimate the asymptotic “retention time” of pollutants, τ , defined as the time taken for the
334 concentration to fall by the factor e^{-1} (DePaul and Sheih, 1985). The normalised values of τ
335 for the WT experiment and the two LESs are given in Table I. For the LES runs, the same
336 analytical model was first fitted to the raw LES time-series (over the time period shown in
337 Figure 2) using the least-squares method (as done in Salizzoni et al. (2009)), and the retention
338 time calculated from its slope. As clearly seen in Figure 2(a), the asymptotic slopes of the
339 LES wash-out curves with the SMAG model are too gentle (i.e. C_a and C_b decay too slowly)
340 compared with the WT data fitted curves. The data in Table I show that normalised retention
341 time is 14% above the WT value, i.e. LES with the SMAG model under-predicts the street
342 canyon ventilation efficiency. Figure 2(b), however, demonstrates that the gradients of the
343 LES wash-out curves with the SB model are in better agreement with the WT data fitted
344 curves; the normalised retention time is now only 3% away from (in this case, below) the WT
345 value. With the inclusion of backscatter in the SGS model, the increased turbulence within
346 the shear layer causes pollutants to be mixed out of the canyon at an earlier time than if
347 backscatter were not included. The fact that the normalised retention time is now slightly too

348 small, i.e. the LES with the SB model slightly over-estimates the street canyon ventilation
 349 efficiency, may be an indication that the backscatter model coefficient is slightly too large.
 350 Finally, the pollutant exchange velocity, v_e , can be calculated from the retention time as
 351 $v_e = H/\tau$. Normalised values of v_e for the WT experiment and each LES are also given in
 352 Table I. Again, the results indicate that v_e is better predicted with the inclusion of backscatter
 353 in the SGS model – the SMAG model value is 12% lower than the WT value, whereas the SB
 354 model value is only 3% higher.

355 **Table I – Normalised asymptotic pollutant retention time, τ , and pollutant exchange**
 356 **velocity, v_e , from the WT experiment, LES with the SMAG model, and LES with the**
 357 **SB model. Each LES value is also given as a % difference from the corresponding WT**
 358 **value.**

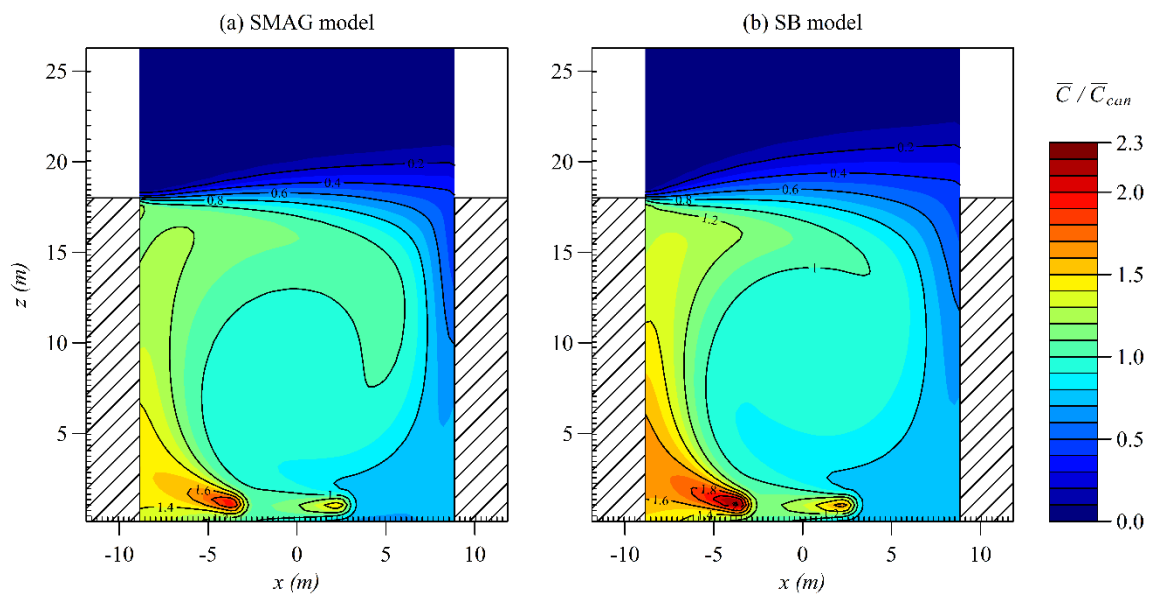
	τ/T	%-diff from WT value	v_e/U_∞	%-diff from WT value
WT	112		0.00893	
SMAG	127	+14 %	0.00786	-12 %
SB	109	-3 %	0.00920	+3 %

359 4.2. Mean 2D fields

360 4.2.1. Pollutant concentration

361 The mean concentration within the street canyon during the last 30 min of simulation, \bar{C}_{can} ,
 362 for each SGS model is given in Table II. \bar{C}_{can} is calculated as the average of C in time and
 363 space for the volume below $z = H$. \bar{C}_{can} is approximately 14% lower with the SB model than
 364 with the SMAG model. This is a direct result of the increased exchange velocity with the
 365 inclusion of backscatter (Section 4.1), which acts to remove pollutants from the canyon more
 366 rapidly (whilst the source strength remains the same). Figure 3 (a) and (b) shows the mean
 367 2D (i.e. time and spanwise average only) concentration fields, \bar{C} , for the SMAG and SB
 368 model, respectively, normalised by \bar{C}_{can} in each case. In both cases, we observe the main
 369 features typical of the mean 2D concentration field as reported in previous wind-tunnel (e.g.
 370 Pavageau and Schatzmann (1999), Simoëns and Wallace (2008), Salizzoni et al. (2009)) and

371 modelling (e.g., Baik and Kim (1999), Liu and Barth (2002)) studies; the released pollutant is
 372 largely transported around the street canyon by the primary recirculation, with some of the
 373 pollutant escaping from the top of the canyon through the roof-level shear layer, resulting in
 374 larger concentrations near the upwind building than near the downwind building. However,
 375 there are also observable differences between the 2D fields for each SGS model, most
 376 notably the vertical extent of the sharp concentration gradient between the street canyon and
 377 the free-stream flow, and the near-source magnitudes. The latter is a consequence of using the
 378 canyon-averaged concentration for normalisation; with more pollutant escaping from the top
 379 of the street canyon with the SB model, the concentration in the lower part of the canyon
 380 relative to the upper part increases. The wider vertical extent of the concentration contours at
 381 roof-level with the SB model is due to the increased turbulent fluctuations causing a locally
 382 faster rate of mixing and thus smoothing out of the concentration gradients there.



383 **Figure 3 – Normalised mean concentration fields, \bar{C} / \bar{C}_{can} , for (a) the SMAG model, and**
 384 **(b) the SB model.**

385 **Table II – Mean concentration within the street canyon, \bar{C}_{can} , for each SGS model, and**
 386 **the % difference**

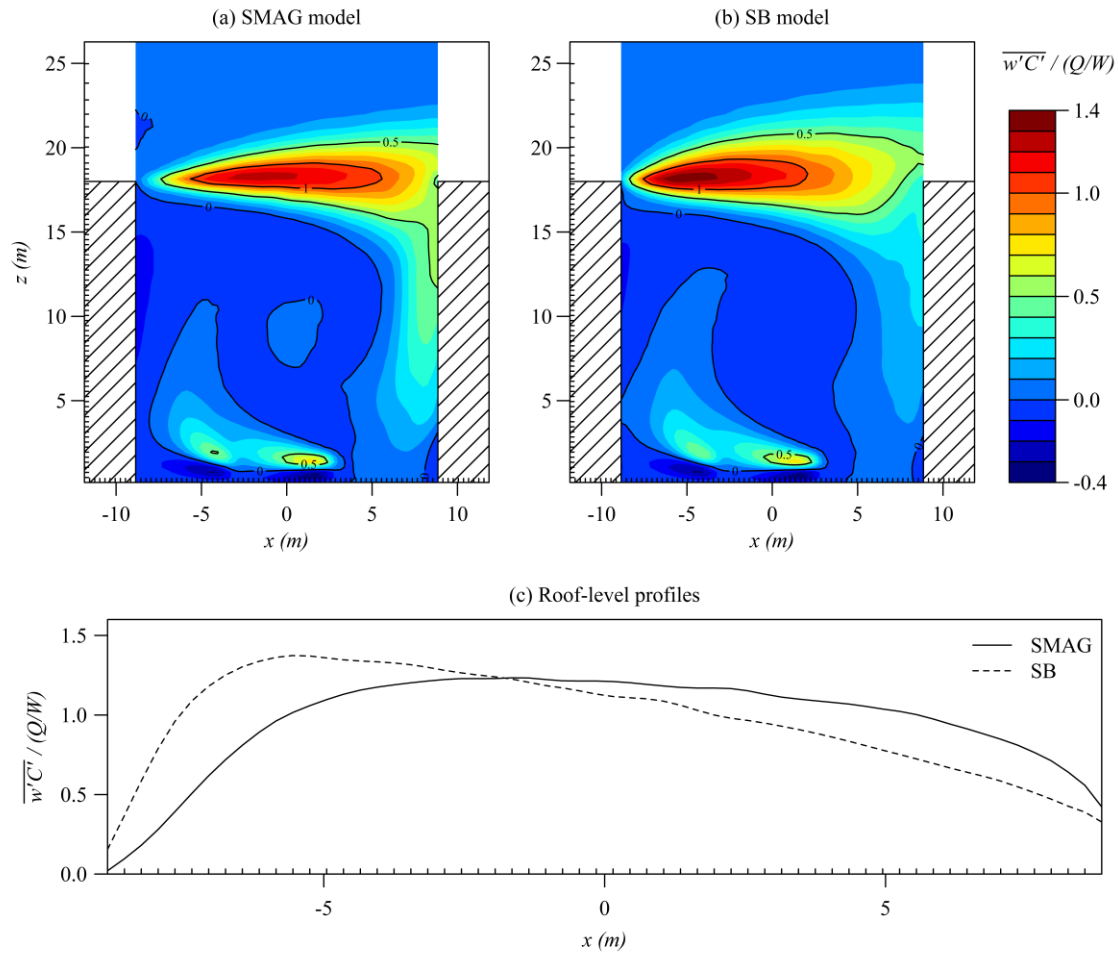
	\bar{C}_{can} ($\mu\text{g m}^{-2}$)	% difference
SMAG	2373	
SB	2031	-14 %

387

388 4.2.2. Turbulent pollutant and momentum flux

389 Figure 4 (a) and (b) shows, for the SMAG and SB model respectively, the mean 2D fields of
390 the vertical pollutant flux by turbulent fluctuations, $\overline{w'C'}$, normalised by the average source
391 flux Q/W , where Q is the total emission rate of the two line sources ($1000 \mu\text{g m}^{-1} \text{s}^{-1}$) and
392 W is the street canyon width (18 m). We also plot in Figure 4 (c) the streamwise profile of
393 normalised $\overline{w'C'_{\text{RL}}}$ for each SGS model, where the subscript RL indicates ‘at roof-level’ (i.e.
394 at $z = H$). During a period of quasi-steady pollutant transport, the total pollutant flux out of
395 the street canyon, i.e. $\overline{wC_{\text{RL}}}$ integrated across roof-level, will be equal to Q/W . Here, we find
396 that the mean value of $\overline{w'C'_{\text{RL}}}/(Q/W)$ across the streamwise profiles is equal to 1.01 for both
397 SGS models. Using a Reynolds decomposition, i.e. taking $w = \bar{w} + w'$ and $C = \bar{C} + C'$,
398 gives $\overline{wC_{\text{RL}}} = \bar{w} \bar{C}_{\text{RL}} + \overline{w'C'_{\text{RL}}}$; our results thus indicate that almost all of the total vertical
399 pollutant flux at roof-level is due to fluctuating velocity (i.e. turbulent processes). Conversely,
400 vertical pollutant flux by mean flow ($\bar{w} \bar{C}_{\text{RL}}$) is small and negative, i.e. its net effect is
401 actually to transport escaped pollutants back into the canyon. This corroborates previous
402 findings, e.g. Baik and Kim (2002), Michioka et al. (2011), while also serving to highlight
403 why RANS models struggle to accurately predict pollutant removal for skimming flow, as
404 they must rely almost entirely on their turbulence parameterisation scheme.

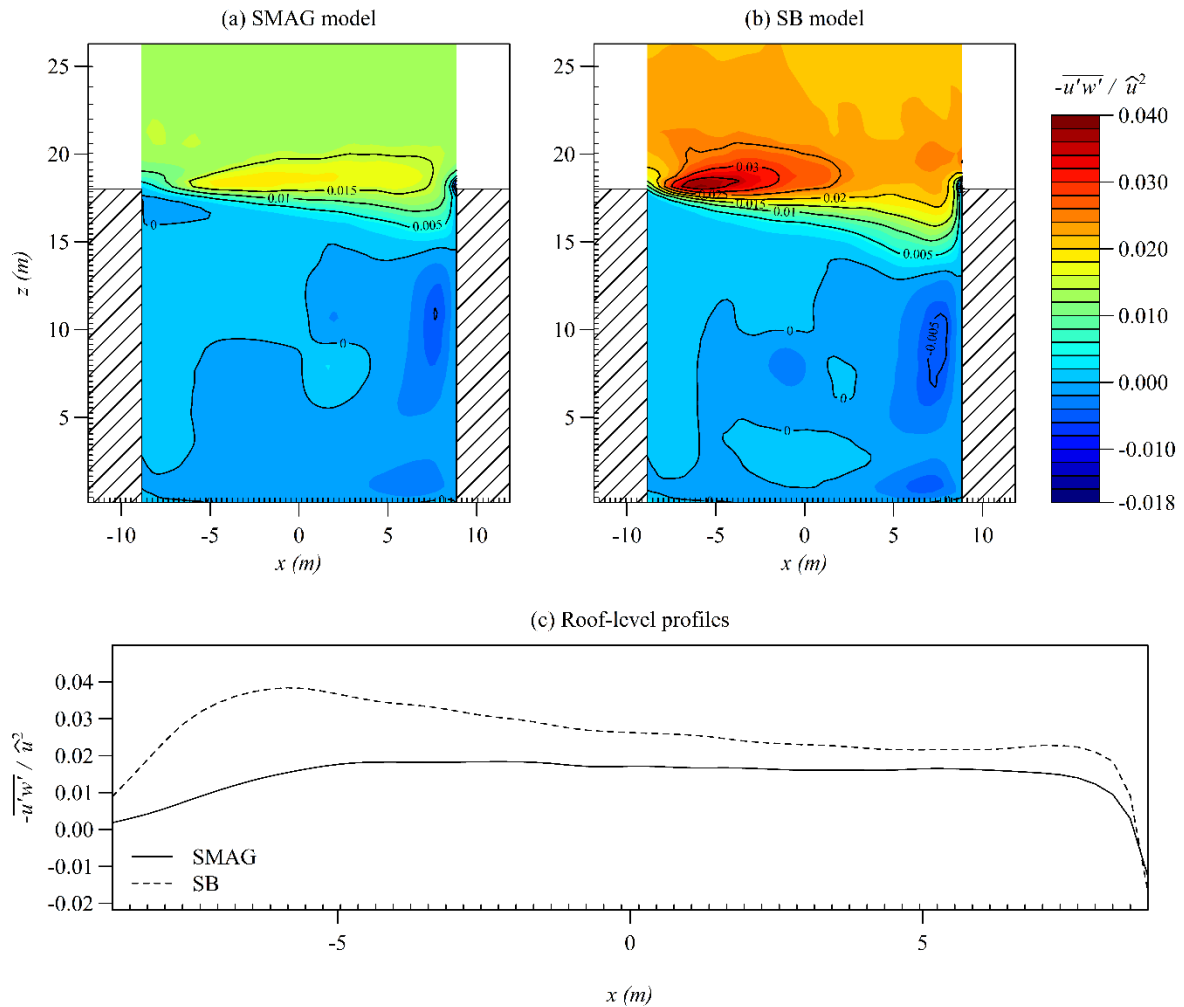
405 We also note from Figure 4 (a) and (b) that the roof-level region of enhanced pollutant flux
406 has a noticeably thicker vertical extent with the SB model than with the SMAG model. For
407 example, the 0.5 contour is approximately 50% thicker along the vertical line passing through
408 the street canyon centre ($x = 0$) with the SB model. Again, this is a consequence of the
409 increased mixing by the backscatter fluctuations which acts to smooth out the gradients of
410 pollutant flux within the shear layer.



411 **Figure 4 – Top panels: Normalised mean fields of vertical pollutant flux by fluctuating**
 412 **velocity, $\overline{w'C'}/(Q/W)$, for (a) the SMAG model, and (b) the SB model. Bottom panel (c)**
 413 **shows the streamwise profile of $\overline{w'C'}/(Q/W)$ at roof-level.**

414 The streamwise roof-level profiles also show that with the SB model, a larger proportion of
 415 the escaping pollutant is predicted to leave the upwind half of the street canyon and,
 416 accordingly, a smaller proportion predicted to leave the downwind half, compared with the
 417 SMAG model – the value of $\overline{w'C'}/(Q/W)_{RL}$ averaged across the upwind half of the street
 418 canyon is around 20% larger with the SB model than with the SMAG model, and thus around
 419 20% smaller across the downwind half. This is because mechanical wind shear is maximum
 420 close to the upwind building corner, where flow separation occurs, and thus local dissipation
 421 ϵ is also large (inspection of the time-averaged dissipation field (not shown) indicates that
 422 roof-level ϵ averaged across the upwind half of the street canyon is around 20% larger than
 423 across the downwind half). Since the local energy backscatter rate is proportional to the local

424 dissipation (Eq. (9)), fluctuating vertical velocity will be more greatly enhanced in the
425 upwind part of the shear layer, leading to a larger pollutant flux there. If we substitute C for
426 u to consider vertical momentum (rather than pollutant) flux, $\overline{w'u'}$, similar behaviour should
427 be expected, since the enhanced vertical velocity fluctuations in the upwind part of the shear
428 layer should act to increase the local momentum exchange between the external flow and the
429 street canyon relative to the downwind part. The 2D fields and roof-level profiles of $-\overline{u'w'}/$
430 $\langle u \rangle^2$ (we follow the convention of plotting the negative of the flux) for each SGS model are
431 plotted in Figure 5. $\langle u \rangle$ in the normalisation factor is the average of \bar{u} between $1 < z/H <$
432 1.5 in the region above the canyon. Note that $-\overline{u'w'}$ averaged across roof-level with each
433 SGS model does not have to be equal in this case. As expected, a comparison between the
434 roof-level profiles obtained with the SMAG and SB model show a greater enhancement of
435 normalised $-\overline{u'w'}$ with the SB model in the upwind half of the street canyon relative to the
436 downwind half.



437 **Figure 5 – As in Figure 4 but for normalised negative vertical momentum flux by**
 438 **fluctuating velocity, $-\overline{u'w'}/\langle u \rangle^2$, where $\langle u \rangle$ is the average of \bar{u} between $1 < z/H < 1.5$**
 439 **in the region above the canyon.**

440

441 4.3. Pollutant exchange rate (PCH)

442 The pollutant exchange rate (PCH), first proposed by Liu et al. (2005), provides an
 443 assessment of the pollutant dilution efficiency of a street canyon. It is typically calculated
 444 alongside the air exchange rate (ACH) (Li et al., 2005; Liu et al., 2005; Cheng et al., 2008),
 445 which describes the rate of air exchange between the street canyon and the free-stream flow
 446 above. It was shown in O'Neill et al. (2016) that the additional grid-scale fluctuations
 447 imparted by the SB model within the roof-level shear layer can cause a significant increase
 448 the air entrainment (removal) rate into (out of) the street canyon, leading to the prediction of

449 a better ventilated street canyon with the SB model than with the SMAG model. For
 450 reference, the time-averaged values of normalised ACH_+ (which is equal to normalised ACH_-
 451 for reasons of mass conservation) for the simulations performed in this study are again
 452 calculated and given in Table III; the SB model value is approximately 60% larger than the
 453 SMAG model value, reconfirming the increased ventilation efficiency predicted with the SB
 454 model. In this paper, we further analyse the effect of the SB model on pollutant dilution
 455 efficiency through the calculation of PCH. Like ACH, PCH (units $\mu\text{g s}^{-1}$), can be separated
 456 into a positive (PCH_+) and negative (PCH_-) part; PCH_+ describes the rate of pollutant
 457 removal from the street canyon, and PCH_- describes the rate of pollutant re-entrainment into
 458 the street canyon (or total entrainment if the background concentration is non-zero). PCH_+ is
 459 calculated as follows:

$$PCH_+(t) = \int_{z=H} w_+(t)C(t)dA, \quad (12)$$

460 where $w(t)$ and $C(t)$ are the instantaneous vertical velocity component and concentration at
 461 time t , respectively, the + subscript implies that only positive values are considered, and A is
 462 the area at the top of the street canyon, at $z = H$. Similarly, PCH_- can be calculated by
 463 substituting $w_-(t)$ (i.e. negative vertical velocities) for $w_+(t)$ in Eq. (12). Unlike ACH, the
 464 difference between positive and negative PCH can be non-zero; in fact, during a period of
 465 quasi-steady pollutant transport, the (time-averaged) difference is expected to be equal to the
 466 total source emission rate $Q_{\text{tot}} = QL_y$ [$\mu\text{g s}^{-1}$] within the LES domain (otherwise the
 467 average concentration within the canyon would not remain steady).

468 The time-averaged values of PCH_+ and PCH_- for each SGS model, normalised by Q_{tot} , are
 469 given in Table III. We note that the difference between $\overline{PCH_+}$ and $\overline{PCH_-}$ in each simulation is
 470 close to, but not exactly, 1. We would expect each value to tend closer to 1 for longer time-
 471 averaging periods (again, here we used 30 minutes). The results indicate that whilst \overline{ACH} is

472 significantly affected by the choice of SGS model (an increase of 60% is observed with the
 473 inclusion of backscatter), $\overline{\text{PCH}}$ is far less affected ($\overline{\text{PCH}}_+$ only increases by 6% with
 474 backscatter). Since we know from the ACH that w_+ increases with the SB model, then in
 475 order for PCH to remain largely unchanged between the SB and SMAG model simulations,
 476 the roof-level concentrations must decrease by an amount that keeps the integral of their
 477 product (w_+C) over A approximately the same. This indicates that PCH, in isolation, provides
 478 insufficient information to assess for changes in the pollutant dilution efficiency of a street
 479 canyon, and should be considered alongside other indicators such as ACH and time-averaged
 480 pollutant concentration.

481 **Table III – Time-averaged normalised air and pollutant exchange rates ($\overline{\text{ACH}}$ and $\overline{\text{PCH}}$)**
 482 **for each SGS model. $V = HWL_y$ is the street canyon volume. $T_{\text{ref}} = H/U_{\text{ref}}$, where U_{ref}**
 483 **is taken as $\bar{u}(z = 1.5H)$ for consistency with O'Neill et al. (2016).**

	$\overline{\text{ACH}}_+/(V/T_{\text{ref}})$	$\overline{\text{PCH}}_+/Q_{\text{tot}}$	$\overline{\text{PCH}}_-/Q_{\text{tot}}$
SMAG	0.05	1.50	0.48
SB	0.08	1.59	0.54

484 5. Conclusions

485 In this study, we have compared two large-eddy simulations of pollutant removal from a
 486 street canyon; one using the widely-adopted Smagorinsky subgrid-scale model, and the other
 487 using a stochastic subgrid-scale model that explicitly accounts for energy backscatter from
 488 the unresolved scales. The SB model had previously been shown to improve the flow
 489 dynamics, and might therefore be used to generate more accurate input parameters for
 490 operational urban dispersion models. The specific case tested was that of neutrally stratified
 491 skimming flow (with perpendicular mean wind) over a nominally two-dimensional street
 492 canyon of unit aspect ratio, with two near-ground-level line sources used to represent two
 493 lanes of continuous traffic emission; this corresponds to an extreme case in which ventilation,
 494 and thus air quality, is poor.

495 The LES output was first validated against wind-tunnel measurements of decaying pollutant
496 concentrations after an emissions shutdown (Salizzoni et al., 2009). It was found that with the
497 inclusion of backscatter, the asymptotic concentration decay rate was in better agreement
498 with the wind-tunnel data. The calculated exchange velocity, v_e , between the canyon and the
499 external flow was around a 15% faster with the SB model, due to the increased mixing within
500 the roof-level shear layer causing a better ventilated street canyon. This result is potentially
501 important for operational models that use an estimate for v_e to describe the mass transfer
502 between the urban canopy and the overlying flow. The steady-state mean concentration
503 within the street canyon was around 15% lower with the SB model owing to the higher-
504 predicted ventilation efficiency.

505 In addition to stochastic backscatter models, there exist other types of SGS model that are
506 able to represent backscatter; for example, nonlinear (or gradient)-type models (Clark et al.,
507 1979; Kosović, 1997). It would be informative to test whether similar predictions of pollutant
508 removal are obtained with such an SGS model to gain further confidence in the importance of
509 backscatter processes in the under-resolved street canyon shear-layer. Finally, we note that
510 the case tested here, although an important example, represents only one of the many street
511 canyon configurations (and atmospheric conditions) found in the real urban canopy layer.
512 Thus, in future work, other configurations should be simulated with the aim of generating a
513 more comprehensive database of look-up parameters (e.g. exchange velocities) to be adopted
514 by operational urban dispersion modellers.

515 **Acknowledgements**

516 We are grateful to the UK Natural Environment Research Council and the English
517 Environment Agency for their financial support of this research. We are also grateful to the
518 anonymous referees for their helpful comments. The computations described herein were

519 performed using the University of Birmingham's BlueBEAR HPC service
520 (<http://www.bear.bham.ac.uk>).

521 **References**

- 522 Baik, J.-J., Kim, J.-J., 1999. A numerical study of flow and pollutant dispersion characteristics in urban
523 street canyons. *Journal of Applied Meteorology*. 38, 1576-1589. doi: 10.1175/1520-
524 0450(1999)038<1576:ANSOFA>2.0.CO;2
- 525 Baik, J.-J., Kim, J.-J., 2002. On the escape of pollutants from urban street canyons. *Atmospheric*
526 *Environment*. 36, 527-536. doi: 10.1016/s1352-2310(01)00438-1
- 527 Baik, J.-J., Park, R.-S., Chun, H.-Y., Kim, J.-J., 2000. A laboratory model of urban street-canyon flows.
528 *Journal of Applied Meteorology*. 39, 1592-1600. doi: 10.1175/1520-
529 0450(2000)039<1592:ALMOUS>2.0.CO;2
- 530 Blackman, K., Perret, L., Savory, E., Piquet, T., 2015. Field and wind tunnel modeling of an idealized
531 street canyon flow. *Atmospheric Environment*. 106, 139-153. doi:
532 10.1016/j.atmosenv.2015.01.067
- 533 Boppana, V.B.L., Xie, Z.T., Castro, I.P., 2010. Large-eddy simulation of dispersion from surface
534 sources in arrays of obstacles. *Boundary-Layer Meteorology*. 135, 433-454. doi:
535 10.1007/s10546-010-9489-9
- 536 Brown, M.J., Lawson, R., Decroix, D., Lee, R., 2000. Mean flow and turbulence measurements around
537 a 2-D array of buildings in a wind tunnel, 11th Joint AMS/AWMA conference on the
538 applications of air pollution, Long Beach, CA, USA.
- 539 Cai, X., 2012. Effects of differential wall heating in street canyons on dispersion and ventilation
540 characteristics of a passive scalar. *Atmospheric Environment*. 51, 268-277. doi:
541 10.1016/j.atmosenv.2012.01.010
- 542 Cai, X.M., Barlow, J.F., Belcher, S.E., 2008. Dispersion and transfer of passive scalars in and above
543 street canyons - Large-eddy simulations. *Atmospheric Environment*. 42, 5885-5895. doi:
544 10.1016/j.atmosenv.2008.03.040
- 545 Cheng, W.C., Liu, C.-H., 2011. Large-eddy simulation of flow and pollutant transports in and above
546 two-dimensional idealized street canyons. *Boundary-Layer Meteorology*. 139, 411-437. doi:
547 10.1007/s10546-010-9584-y
- 548 Cheng, W.C., Liu, C.-H., Leung, D.Y.C., 2008. Computational formulation for the evaluation of street
549 canyon ventilation and pollutant removal performance. *Atmospheric Environment*. 42, 9041-
550 9051. doi: 10.1016/j.atmosenv.2008.09.045
- 551 Cheng, W.C., Porte-Agel, F., 2015. Adjustment of turbulent boundary-layer flow to idealized urban
552 surfaces: A large-eddy simulation study. *Boundary-Layer Meteorology*. 155, 249-270. doi:
553 10.1007/s10546-015-0004-1
- 554 Clark, R.A., Ferziger, J.H., Reynolds, W., 1979. Evaluation of subgrid-scale models using an accurately
555 simulated turbulent flow. *Journal of Fluid Mechanics*. 91, 1-16. doi:
556 10.1017/S002211207900001X
- 557 Coceal, O., Thomas, T.G., Castro, I.P., Belcher, S.E., 2006. Mean flow and turbulence statistics over
558 groups of urban-like cubical obstacles. *Boundary-Layer Meteorology*. 121, 491-519. doi:
559 10.1007/s10546-006-9076-2
- 560 Cui, Z.Q., Cai, X.M., Baker, C.J., 2004. Large-eddy simulation of turbulent flow in a street canyon.
561 *Quarterly Journal of the Royal Meteorological Society*. 130, 1373-1394. doi:
562 10.1256/qj.02.150
- 563 Dejoan, A., Santiago, J.L., Martilli, A., Martin, F., Pinelli, A., 2010. Comparison between large-eddy
564 simulation and Reynolds-averaged Navier-Stokes computations for the MUST field

565 experiment. Part II: Effects of incident wind angle deviation on the mean flow and plume
566 dispersion. *Boundary-Layer Meteorology*. 135, 133-150. doi: 10.1007/s10546-010-9467-2
567 DePaul, F.T., Sheih, C.M., 1985. A tracer study of dispersion in an urban street canyon. *Atmospheric*
568 *Environment*. 19, 555-559. doi: 10.1016/0004-6981(85)90034-4
569 Di Bernardino, A., Monti, P., Leuzzi, G., Querzoli, G., 2015. Water-channel study of flow and
570 turbulence past a two-dimensional array of obstacles. *Boundary-Layer Meteorology*. 155,
571 73-85. doi: 10.1007/s10546-014-9987-2
572 Germano, M., Piomelli, U., Moin, P., Cabot, W.H., 1991. A dynamic subgrid-scale eddy viscosity
573 model. *Physics of Fluids A-Fluid Dynamics*. 3, 1760-1765. doi: 10.1063/1.857955
574 Kastner-Klein, P., Plate, E.J., 1999. Wind-tunnel study of concentration fields in street canyons.
575 *Atmospheric Environment*. 33, 3973-3979. doi: 10.1016/s1352-2310(99)00139-9
576 Kosović, B., 1997. Subgrid-scale modelling for the large-eddy simulation of high-Reynolds-number
577 boundary layers. *Journal of Fluid Mechanics*. 336, 151-182. doi:
578 10.1017/s0022112096004697
579 Letzel, M.O., Krane, M., Raasch, S., 2008. High resolution urban large-eddy simulation studies from
580 street canyon to neighbourhood scale. *Atmospheric Environment*. 42, 8770-8784. doi:
581 10.1016/j.atmosenv.2008.08.001
582 Li, X.-X., Leung, D.Y.C., Liu, C.-H., Lam, K.M., 2008. Physical modeling of flow field inside urban street
583 canyons. *Journal of Applied Meteorology and Climatology*. 47, 2058-2067. doi:
584 10.1175/2007jamc1815.1
585 Li, X.-X., Liu, C.-H., Leung, D.Y.C., Lam, K.M., 2006. Recent progress in CFD modelling of wind field
586 and pollutant transport in street canyons. *Atmospheric Environment*. 40, 5640-5658. doi:
587 10.1016/j.atmosenv.2006.04.055
588 Li, X.X., Liu, C.H., Leung, D.Y.C., 2005. Development of a $k-\epsilon$ model for the determination of air
589 exchange rates for street canyons. *Atmospheric Environment*. 39, 7285-7296. doi:
590 10.1016/j.atmosenv.2005.09.007
591 Lilly, D.K., 1992. A proposed modification of the Germano subgrid-scale closure method. *Physics of*
592 *Fluids A*. 4, 633-635. doi: 10.1063/1.858280
593 Liu, C.-H., Wong, C.C.C., 2014. On the pollutant removal, dispersion, and entrainment over two-
594 dimensional idealized street canyons. *Atmospheric Research*. 135, 128-142. doi:
595 10.1016/j.atmosres.2013.08.006
596 Liu, C.H., Barth, M.C., 2002. Large-eddy simulation of flow and scalar transport in a modeled street
597 canyon. *Journal of Applied Meteorology*. 41, 660-673. doi: 10.1175/1520-
598 0450(2002)041<0660:lesofa>2.0.co;2
599 Liu, C.H., Leung, D.Y.C., Barth, M.C., 2005. On the prediction of air and pollutant exchange rates in
600 street canyons of different aspect ratios using large-eddy simulation. *Atmospheric*
601 *Environment*. 39, 1567-1574. doi: 10.1016/j.atmosenv.2004.08.036
602 Mason, P.J., 1994. Large-eddy simulation - A critical-review of the technique. *Quarterly Journal of*
603 *the Royal Meteorological Society*. 120, 1-26. doi: 10.1002/qj.49712051503
604 Mason, P.J., Callen, N.S., 1986. On the magnitude of the subgrid-scale eddy coefficient in large-eddy
605 simulations of turbulent channel flow. *Journal of Fluid Mechanics*. 162, 439-462. doi:
606 10.1017/s0022112086002112
607 Mason, P.J., Thomson, D.J., 1992. Stochastic backscatter in large-eddy simulations of boundary-
608 layers. *Journal of Fluid Mechanics*. 242, 51-78. doi: 10.1017/s0022112092002271
609 Meroney, R.N., Pavageau, M., Rafailidis, S., Schatzmann, M., 1996. Study of line source
610 characteristics for 2-D physical modelling of pollutant dispersion in street canyons. *Journal of*
611 *Wind Engineering and Industrial Aerodynamics*. 62, 37-56. doi: 10.1016/s0167-
612 6105(96)00057-8
613 Michioka, T., Sato, A., Takimoto, H., Kanda, M., 2011. Large-eddy simulation for the mechanism of
614 pollutant removal from a two-dimensional street canyon. *Boundary-Layer Meteorology*. 138,
615 195-213. doi: 10.1007/s10546-010-9556-2

616 O'Neill, J.J., Cai, X.-M., Kinnersley, R., 2015. A generalised stochastic backscatter model: large-eddy
617 simulation of the neutral surface layer. *Quarterly Journal of the Royal Meteorological Society*.
618 141, 2617-2629. doi: 10.1002/qj.2548

619 O'Neill, J.J., Cai, X.-M., Kinnersley, R., 2016. Improvement of a stochastic backscatter model and
620 application to large-eddy simulation of street canyon flow. *Quarterly Journal of the Royal*
621 *Meteorological Society*. 142, 1121-1132. doi: 10.1002/qj.2715

622 Oke, T.R., 1987. *Boundary Layer Climates*, Second Edition. Methuen, London, UK.

623 Oke, T.R., 1988. Street design and urban canopy layer climate. *Energy and buildings*. 11, 103-113. doi:
624 10.1016/0378-7788(88)90026-6

625 Park, S.B., Baik, J.J., 2013. A large-eddy simulation study of thermal effects on turbulence coherent
626 structures in and above a building array. *Journal of Applied Meteorology and Climatology*. 52,
627 1348-1365. doi: 10.1175/jamc-d-12-0162.1

628 Pavageau, M., Schatzmann, M., 1999. Wind tunnel measurements of concentration fluctuations in
629 an urban street canyon. *Atmospheric Environment*. 33, 3961-3971. doi: 10.1016/S1352-
630 2310(99)00138-7

631 Pielke, R., Cotton, W., Walko, R., Tremback, C., Lyons, W., et al., 1992. A comprehensive
632 meteorological modeling system—RAMS. *Meteorology and Atmospheric Physics*. 49, 69-91.
633 doi: 10.1007/BF01025401

634 Salim, S.M., Buccolieri, R., Chan, A., Di Sabatino, S., 2011a. Numerical simulation of atmospheric
635 pollutant dispersion in an urban street canyon: Comparison between RANS and LES. *Journal*
636 *of Wind Engineering and Industrial Aerodynamics*. 99, 103-113. doi:
637 10.1016/j.jweia.2010.12.002

638 Salim, S.M., Cheah, S.C., Chan, A., 2011b. Numerical simulation of dispersion in urban street canyons
639 with avenue-like tree plantings: Comparison between RANS and LES. *Build. Environ*. 46,
640 1735-1746. doi: 10.1016/j.buildenv.2011.01.032

641 Salizzoni, P., Soulhac, L., Mejean, P., 2009. Street canyon ventilation and atmospheric turbulence.
642 *Atmospheric Environment*. 43, 5056-5067. doi: 10.1016/j.atmosenv.2009.06.045

643 Salizzoni, P., Soulhac, L., Mejean, P., Perkins, R., 2008. Influence of a Two-scale Surface Roughness on
644 a Neutral Turbulent Boundary Layer. *Boundary-Layer Meteorology*. 127, 97-110. doi:
645 10.1007/s10546-007-9256-8

646 Santiago, J.L., Dejoan, A., Martilli, A., Martin, F., Pinelli, A., 2010. Comparison between large-eddy
647 simulation and Reynolds-averaged Navier-Stokes computations for the MUST field
648 experiment. Part I: Study of the flow for an incident wind directed perpendicularly to the
649 front array of containers. *Boundary-Layer Meteorology*. 135, 109-132. doi: 10.1007/s10546-
650 010-9466-3

651 Simoëns, S., Wallace, J.M., 2008. The flow across a street canyon of variable width—Part 2: Scalar
652 dispersion from a street level line source. *Atmospheric Environment*. 42, 2489-2503. doi:
653 10.1016/j.atmosenv.2007.12.013

654 Smagorinsky, J., 1963. General circulation experiments with the primitive equations. *Monthly*
655 *Weather Review*. 91, 99-164. doi: 10.1175/1520-0493(1963)091<0099:gcewtp>2.3.co;2

656 Tominaga, Y., Stathopoulos, T., 2010. Numerical simulation of dispersion around an isolated cubic
657 building: Model evaluation of RANS and LES. *Build. Environ*. 45, 2231-2239. doi:
658 10.1016/j.buildenv.2010.04.004

659 Vardoulakis, S., Fisher, B.E.A., Pericleous, K., Gonzalez-Flesca, N., 2003. Modelling air quality in street
660 canyons: a review. *Atmospheric Environment*. 37, 155-182. doi: 10.1016/s1352-
661 2310(02)00857-9

662 Walton, A., Cheng, A.Y.S., 2002. Large-eddy simulation of pollution dispersion in an urban street
663 canyon - Part II: idealised canyon simulation. *Atmospheric Environment*. 36, 3615-3627. doi:
664 10.1016/s1352-2310(02)00260-1

665 WHO, 2015. *World health statistics 2015*. World Health Organization, Printed in Luxembourg.

666 Xie, S., Zhang, Y., Qi, L., Tang, X., 2003. Spatial distribution of traffic-related pollutant concentrations
667 in street canyons. *Atmospheric Environment*. 37, 3213-3224. doi: 10.1016/S1352-
668 2310(03)00321-2

669 Xie, Z., Voke, P., Hayden, P., Robins, A., 2004. Large-eddy simulation of turbulent flow over a rough
670 surface. *Boundary-Layer Meteorology*. 111, 417-440. doi:
671 10.1023/b:boun.0000016599.75196.17

672 Xie, Z.T., Castro, I.P., 2006. LES and RANS for turbulent flow over arrays of wall-mounted obstacles.
673 *Flow Turbulence and Combustion*. 76, 291-312. doi: 10.1007/s10494-006-9018-6

674

675